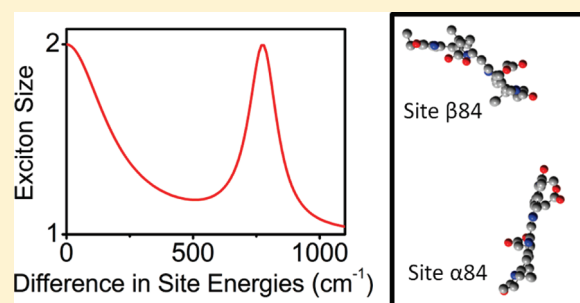


Vibronic Enhancement of Exciton Sizes and Energy Transport in Photosynthetic Complexes

Jordan M. Womick and Andrew M. Moran*

Department of Chemistry, The University of North Carolina at Chapel Hill, Chapel Hill, North Carolina 27599, United States

ABSTRACT: Transport processes and spectroscopic phenomena in light harvesting proteins depend sensitively on the characteristics of electron–phonon couplings. Decoherence imposed by low-frequency nuclear motion generally suppresses the delocalization of electronic states, whereas the Franck–Condon progressions of high-frequency intramolecular modes underpin a hierarchy of vibronic Coulombic interactions between pigments. This Article investigates the impact of vibronic couplings on the electronic structures and relaxation mechanisms of two cyanobacterial light-harvesting proteins, allophycocyanin (APC) and C-phycocyanin (CPC). Both APC and CPC possess three pairs of pigments (i.e., dimers) that undergo electronic relaxation on the subpicosecond time scale. Electronic relaxation is ~ 10 times faster in APC than in CPC despite the nearly identical structures of their pigment dimers. We suggest that the distinct behaviors of these closely related proteins are understood on the same footing only in a basis of joint electronic-nuclear states (i.e., vibronic excitons). A vibronic exciton model predicts well-defined rate enhancements in APC at realistic values of the site reorganization energies, whereas a purely electronic exciton model points to faster dynamics in CPC. Calculated exciton sizes (i.e., participation ratios) show that wave function delocalization underlies the rate enhancement predicted by the vibronic exciton model. Strong vibronic coupling and heterogeneity in the pigment sites are the key ingredients of the vibronic delocalization mechanism. In contrast, commonly employed purely electronic exciton models see heterogeneity as only a localizing influence. This work raises the possibility that similar vibronic effects, which are often neglected, may generally have a significant influence on energy transport in molecular aggregates and photosynthetic complexes.



I. INTRODUCTION

Spectroscopy and dynamics in molecular aggregates and light-harvesting proteins are intimately connected to interactions between electronic and nuclear coordinates.^{1–15} In these systems, low-frequency thermally driven nuclear motion generally constitutes a source of noise responsible for decoherence between molecular sites. Vibronic couplings in high-frequency quantized modes, while not thermally populated, also influence exciton localization by reducing the magnitudes of molecular transition dipoles at their electronic origins, which, in turn, suppresses interactions between sites. The treatment of high-frequency modes with large displacements (i.e., with large reorganization energies) generally differs in investigations of molecular aggregates and semiconductor organic crystals. Vibronic exciton models, for example, define electronic structure in a basis of vibronic levels in systems whose optical spectra exhibit extended Franck–Condon progressions (e.g., acene crystals).^{16–20} Vibronic excitations are allowed to delocalize between sites, and the relationship between intramolecular reorganization energy and intermolecular coupling is naturally accounted for. Alternative approaches use the spectral density of the system's phonon environment to handle quantized modes with moderate Huang–Rhys factors. Low-frequency motions are then seen to promote transitions between electronic states whose energy differences are small compared with $k_B T$, whereas the quantized modes

enable energy conservation in fast transitions between electronic states with large energy gaps. Examples of transitions assisted by quantized modes (i.e., promoting modes) are found in photosynthetic reaction centers.^{21–23}

The present Article is motivated by our ongoing efforts to understand the origin of the difference in electronic relaxation rates observed in the pigment dimers of allophycocyanin (APC) and C-phycocyanin (CPC).^{24–26} Figure 1 shows the structures of the dimers in APC and CPC isolated from *Spirulina platensis*.^{27,28} The intermolecular distances (2.05 nm) and relative molecular orientations are quite similar in the two systems; the angles between transition dipoles are $\sim 55^\circ$.^{24,25,29,30} The geometries of the $\beta 84$ pigments are nearly indistinguishable, whereas slight differences are found at the $\alpha 84$ sites. As shown in Figure 1, the BD and CD inter-ring torsion angles are $>25^\circ$ larger in CPC, which may influence electronic structure by interrupting double-bond conjugation. Despite these structural similarities, our transient absorption anisotropy experiments yield electronic population transfer time constants of 220 and 970 fs in APC and CPC, respectively. In addition, 2D photon echo experiments provide clear evidence of sub-20 fs population transfer in APC; this

Received: July 19, 2010

Revised: December 20, 2010

Published: January 26, 2011

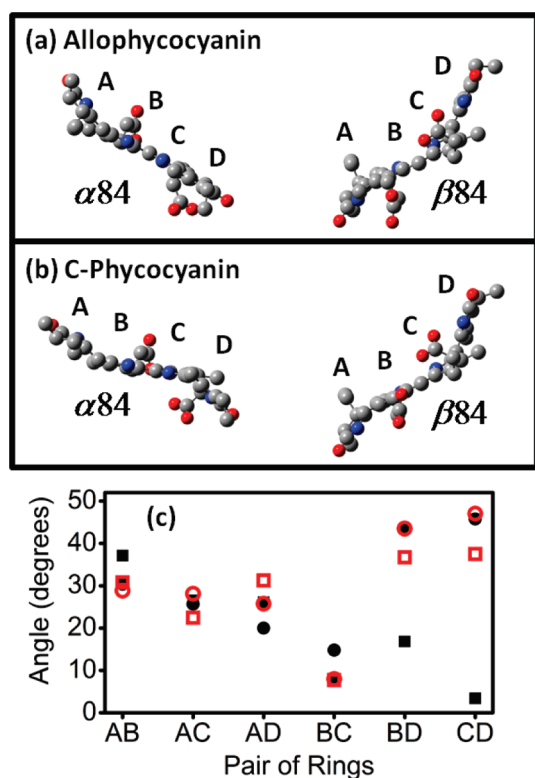


Figure 1. (a) Structure of APC dimer generated using PDB file 1ALL.²⁷ (b) Structure of CPC dimer generated using PDB file 1GH0.²⁸ X-ray data for both systems are obtained using proteins isolated from *Spirulina platensis*. The intermolecular distances are 2.06 and 2.01 nm for APC and CPC, respectively. (c) Inter-ring torsion angles for $\alpha 84$ in APC (filled black squares), $\beta 84$ in APC (filled black circles), $\alpha 84$ in CPC (open red squares), and $\beta 84$ in CPC (open red circles). In this convention, ring A is covalently bonded to a cysteine residue.

nonradiative transition also imposes significant lifetime broadening in the linear absorption spectrum of APC.²⁴ The faster relaxation process in APC is surprising given that the difference in $\alpha 84$ and $\beta 84$ site energies (760 cm^{-1}) is over twice that found in CPC (350 cm^{-1}). We remark that our conclusions are, more or less, consistent with previous experimental studies of these two proteins isolated from different organisms, which have proven to be essential to the interpretation of our experiments.^{29–38}

In this contribution, we investigate electronic relaxation mechanisms in APC and CPC using modified Redfield theory with the goal of understanding the dynamics in both systems on a common footing.^{39,40} Modified Redfield theory is appropriate for this task because of its ability to interpolate between the limits of weak electron–phonon coupling (i.e., Redfield limit)⁴¹ and weak donor–acceptor interactions (i.e., Förster limit).⁴² Our fitting of spectroscopic line widths in APC and CPC yields site reorganization energies ranging from 235 to 417 cm^{-1} , whereas the intermolecular couplings in both systems are approximately 150 cm^{-1} . The comparable magnitudes of these two quantities make clear the need for a model capable of handling the intermediate coupling regime. The main focus of this work is the exploration of kinetic effects associated with a strongly coupled hydrogen out-of-plane (HOOP) wagging vibration, which gives rise to pronounced recurrences in the transient absorption anisotropies of both systems.^{24,25} The HOOP mode

is of particular interest because its 800 cm^{-1} frequency closely matches the energy gap between electronic states in APC but not in CPC. We suggested that the HOOP vibration functions in APC as the promoting mode responsible for extremely rapid relaxation between exciton states.²⁴ In contrast, the relaxation rate of CPC agrees well with the predictions of Förster theory.³⁰ In addition, the localized basis is adequate for the interpretation of spectroscopic signals in CPC.^{25,26} Below, it is shown that the behavior of both systems can be understood in a consistent manner by explicitly treating vibronic excitations of the HOOP mode as part of the system rather than the bath.

II. MODEL HAMILTONIANS USED IN RATE CALCULATIONS

This Section presents the two classes of Frenkel exciton models employed in this work. Background on these models and the latest developments can be found in recent literature.^{5,18,40,43–45} In the first model, population transfer dynamics are computed in a basis of purely electronic two-level systems whose spectral densities possess all information on vibronic couplings. The second model incorporates vibronic levels in the system Hamiltonian instead of the bath. Vibronic exciton models are often used to describe electronic structure in molecular crystals such as tetracene, where the individual sites exhibit well-resolved Franck–Condon progressions.^{46,47} Applications have also been made to polypeptides,^{48,49} the antenna of purple bacteria,⁵⁰ and molecular aggregates.^{51,52}

In both models considered here, the Hamiltonian of the pigment complex is partitioned into three components as

$$H = H_{\text{Sys}} + H_{\text{Bath}} + H_{\text{Sys} - \text{Bath}} \quad (1)$$

Sections IIA and IIB present two different partitioning schemes, which differ in whether the intramolecular HOOP mode is treated as part of the system or bath. The bath is described within the well-known Brownian oscillator (BO) framework for which the key equations are summarized in the Appendix.^{43,53} The BO model views both intramolecular and intermolecular modes as displaced harmonic oscillators. The two types of coordinates are distinguished only in the rates at which they dissipate energy following electronic excitation of the system. It is shown below that the partitioning scheme has nontrivial consequences on both transport kinetics and the predicted exciton sizes.

IIA. Purely Electronic Exciton Model. The model presented in this Section (and in Section IIB) is specific to the pigment dimers found in APC and CPC. However, the formulas are written using restricted summations to allow straightforward generalization to systems possessing additional pigments and/or larger Huang–Rhys factors, or both. With all nuclear modes kept as part of the bath, the system Hamiltonian is given by^{5,43}

$$H_{\text{Sys}}^{\text{el}} = \sum_{m=1}^2 E_m B_m^{\dagger} B_m + \sum_{m=1}^2 \sum_{n \neq m}^2 J_{mn} B_m^{\dagger} B_n \quad (2)$$

where the basis is composed of purely electronic two-level systems. Here E_m is the thermally averaged energy gap of pigment m at the ground-state equilibrium geometry (i.e., Franck–Condon geometry) and J_{mn} is the Coulombic coupling between molecules m and n . The Heitler–London approximation has been made in writing $H_{\text{Sys}}^{\text{el}}$, which contains only interactions between states

with the same number of excitations. Quartic resonant interactions between chromophores are neglected because they are generally small compared with the quadratic coupling, J_{mn} . Moreover, the off-resonant terms found in the generalized Frenkel exciton Hamiltonian are neglected in $H_{\text{Sys}}^{\text{el}}$ because $J_{mn} \ll E_m$ in both APC and CPC.⁴³

The bath possesses two primary BO coordinates in the present purely electronic exciton model. First, interactions with low-frequency motions of the environment at site m are accounted for with an overdamped BO coordinate for which the odd component of the spectral density is written as⁵³

$$C_m^{\text{OD}}(\omega) = 2\lambda_m \frac{\omega \Lambda_m}{\omega^2 + \Lambda_m^2} \quad (3)$$

For APC and CPC, $C_m^{\text{OD}}(\omega)$ peaks at frequencies smaller than $k_B T$ because the site reorganization energy, λ_m , is large compared with the relaxation rate, Λ_m . In this slow modulation regime, the standard deviation of fluctuations in E_m is (approximately) given by $(2\lambda_m k_B T)^{1/2}$.⁵³ The second primary oscillator represents the underdamped intramolecular HOOP mode using the spectral density⁵³

$$C_m^{\text{UD}}(\omega) = S_m \Omega_m^2 [\delta(\omega - \Omega_m) - \delta(\omega + \Omega_m)] \quad (4)$$

where S_m and $S_m \Omega_m$ are, respectively, the Huang–Rhys factor and reorganization energy at site m . It is adequate to write $C_m^{\text{UD}}(\omega)$ using delta functions instead of functions with finite widths because the solvent reorganization energy is large compared with the line widths of intramolecular modes. In all simulations conducted below, the mode frequency and displacement are taken to be equivalent on both pigment sites in the dimer. The total odd component of the spectral density at site m is given by the sum of these two contributions

$$C_m(\omega) = C_m^{\text{OD}}(\omega) + C_m^{\text{UD}}(\omega) \quad (5)$$

The line broadening function at site m is then computed using⁵³

$$g_m(t) = \frac{1}{2\pi} \int_{-\infty}^{\infty} d\omega \frac{1 - \cos(\omega t)}{\omega^2} \coth(\beta \hbar \omega / 2) C_m(\omega) + \frac{i}{2\pi} \int_{-\infty}^{\infty} d\omega \frac{\sin(\omega t) - \omega t}{\omega^2} C_m(\omega) \quad (6)$$

Because of the $\coth(\beta \hbar \omega / 2)$ function in eq 6, the low-frequency portion of $C_m^{\text{OD}}(\omega)$ dominates the real part of $g_m(t)$ and is therefore primarily responsible for spectroscopic line broadening. In contrast, $C_m^{\text{UD}}(\omega)$ contributes mainly to the imaginary part of $g_m(t)$ because the frequency of the HOOP is over three times larger than $k_B T$. Overall, optical spectra computed with $g_m(t)$ appear as vibronic progressions in which the individual transitions exhibit identical line widths determined by $C_m^{\text{OD}}(\omega)$. Assuming that each site possesses an uncorrelated bath, the transformation of the local line broadening functions into the single exciton basis is given by

$$g_{abcd}(t) = \sum_{n=1}^2 \phi_{an} \phi_{bn} \phi_{cn} \phi_{dn} g_n(t) \quad (7)$$

where the eigenvector of exciton state a is written as

$$|a\rangle = \sum_{m=1}^2 \phi_{am} |m\rangle \quad (8)$$

IIB. Vibronic Exciton Model. As an alternative to the above approach, vibronic interactions may be incorporated explicitly using the Holstein-like Hamiltonian^{17,18,54}

$$H_{\text{Sys}}^{\text{vb}} = \sum_{m=1}^2 \sum_{\nu=0}^1 (E_m + \nu \hbar \omega_{\nu}) B_{m\nu}^{\dagger} B_{m\nu} + \sum_{m=1}^2 \sum_{n \neq m}^2 \sum_{\nu=0}^1 \sum_{\sigma=0}^1 J_{mn} B_{m\nu}^{\dagger} B_{n\sigma} \langle 0|\nu\rangle \langle 0|\sigma\rangle \quad (9)$$

where the indices m and n represent molecular sites, ν and σ are vibronic levels at sites m and n , and ω_{ν} is the frequency of an intramolecular mode. In this notation, the operator $B_{m\nu}^{\dagger}$ ($B_{m\nu}$) creates (annihilates) an excitation at molecule m in vibronic level ν . $H_{\text{Sys}}^{\text{vb}}$ treats only the intramolecular HOOP mode of APC and CPC explicitly. The product of overlap integrals between nuclear wave functions, $\langle 0|\nu\rangle \langle 0|\sigma\rangle$, distributes the intersite Coulombic coupling, J_{mn} , in the vibronic basis; these integrals are computed in a harmonic basis with no Duchinsky rotation.⁵⁵ The expansion in vibronic levels is truncated at $\nu = 1$ because the overlap integrals, $\langle 0|\nu\rangle$, become negligible for higher excitation quanta, ν , due to the modest Huang–Rhys factors of APC and CPC.^{24,25}

In this vibronic exciton model, each pigment site is coupled to a single overdamped BO coordinate under the assumption that all vibronic levels associated with a particular pigment site experience the same bath-induced fluctuations. The total spectral density at site m is then equal to $C_m^{\text{OD}}(\omega)$. The single exciton block of the Hamiltonian matrix is constructed in a basis of vibronic excitations denoted as $|m, \nu\rangle$, which upon diagonalization yields

$$|a\rangle = \sum_{m=1}^2 \sum_{\nu=0}^1 \phi_{a,m\nu} |m, \nu\rangle \quad (10)$$

Transformation of the line broadening functions from the local to exciton basis is achieved with

$$g_{abcd}(t) = \sum_{n=1}^2 \sum_{\nu=0}^1 \phi_{a,n\nu} \phi_{b,n\nu} \phi_{c,n\nu} \phi_{d,n\nu} g_n(t) \quad (11)$$

where $g_m(t)$ is defined in eq 6. Figure 2 summarizes the key ideas involved in the partitioning schemes utilized in the purely electronic and vibronic exciton Hamiltonians.

The coherent exciton scattering (CES) formalism is a powerful Green function approach that has been used to simulate the optical response and delocalization of excitons in molecular aggregates.^{13,56,57} The physical picture adopted by the present model is quite similar to CES. As in CES, the $g_m(t)$, which accounts for thermally driven motion, imparts identical fluctuations on all vibronic levels, ν , of the individual pigments. The purely electronic exciton model differs in that intramolecular modes can also influence the line widths through the real part of $g_m(t)$, where the importance of this contribution increases with decreasing mode frequency. We also remark that both our vibronic exciton model and CES account for only the ground vibrational level in the electronic ground state.⁵⁷ For this reason, E_m represents the electronic origin (i.e., 0–0 transition) when $H_{\text{Sys}}^{\text{vb}}$ is employed.

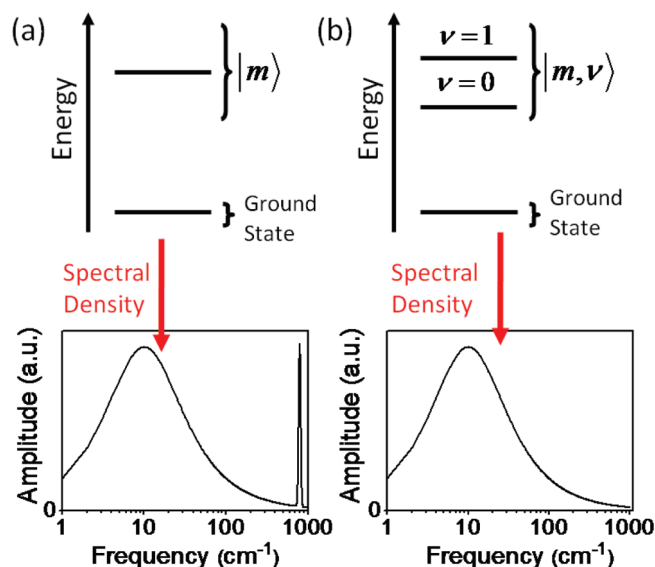


Figure 2. Key ideas involved in the Frenkel exciton models presented in Section II. (a) Exciton model corresponding to $H_{\text{Sys}}^{\text{el}}$. The system Hamiltonian is diagonalized in a basis of two-level systems, and underdamped modes are incorporated in the spectral density using $C_m^{\text{UD}}(\omega)$. The resonance at 800 cm⁻¹ has been given a finite spectral width for illustration. (b) Vibronic exciton Hamiltonian, $H_{\text{Sys}}^{\text{vb}}$, explicitly treats intramolecular modes with large Franck–Condon factors. The spectral density possesses contributions from only the overdamped nuclear motion described by $C_m^{\text{OD}}(\omega)$.

II.C. Modified Redfield Rate Constants. The modified Redfield rate constants corresponding to a transition initiating in exciton *a* and terminating in exciton *b* is computed using³⁹

$$K_{ba} = 2\text{Re} \int_0^\infty dt F_{ba}(t) \exp[-i(\omega_b - \omega_a)t - g_{bbb}(t) - g_{aaa}^*(t) + 2\{g_{bbaa}(t) + i(\lambda_{bbaa} - \lambda_{aaaa})t\}] \quad (12)$$

where

$$F_{ba}(t) = [\dot{g}_{baab}(t) - \{\dot{g}_{abaa}(t) - \dot{g}_{abbb}(t) + 2i\lambda_{abaa}\} \{\dot{g}_{aaba}(t) - \dot{g}_{bbba}(t) + 2i\lambda_{baaa}\}] \quad (13)$$

General physical insights associated with modified Redfield theory have been discussed in recent reviews.^{5,40,43} Ref 40 demonstrates the ability of modified Redfield theory to interpolate between the limits of weak (Redfield) and strong (Förster) system–bath interactions. In addition, modified Redfield theory is capable of capturing rate enhancements involving the exchange of multiple excitation quanta with the bath. In contrast, traditional Redfield theory accounts only for transitions through vibronic channels in which the initial and final phonon states differ by single excitation quanta.

III. RESULTS AND DISCUSSION

Electronic population transfer rates in APC and CPC are computed below using the two classes of system Hamiltonians presented in Section II. This comparison of models focuses on the appropriate treatment of the strongly coupled HOOP mode at 800 cm⁻¹. As suggested by Figure 2, $H_{\text{Sys}}^{\text{el}}$ keeps the HOOP coordinate as a part of the spectral density, which allows it to function as a traditional promoting mode in an internal

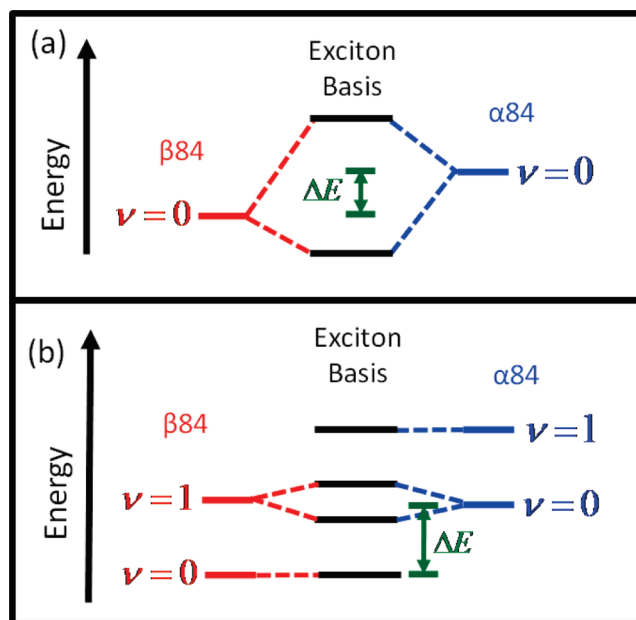


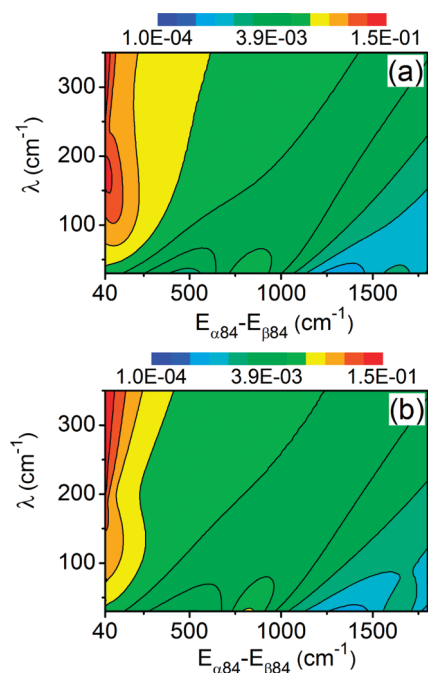
Figure 3. Energy level diagrams illustrating the electronic structures associated with (a) $H_{\text{Sys}}^{\text{el}}$ and (b) $H_{\text{Sys}}^{\text{vb}}$ for the molecular dimers in APC and CPC. Only the excited states of the system are shown because both Hamiltonians have block diagonal form. The difference in site energies is $\Delta E = E(\alpha 84) - E(\beta 84)$. (a) For $H_{\text{Sys}}^{\text{el}}$, the intersite coupling, $J_{\alpha 84, \beta 84}$, reflects only the transition dipoles for the electronic origins. (b) Each site has two vibronic levels through which exciton delocalization can occur. Dashed lines signify the basis states that contribute most to the respective excitons when $\Delta E \approx \hbar\omega$ and $J_{\alpha 84, \beta 84} < \Delta E$.

conversion process. In contrast, $H_{\text{Sys}}^{\text{vb}}$ handles explicitly the partitioning of the transition dipole in the vibronic progression of the HOOP mode, thereby supporting a mechanism of intersite wave function delocalization not present in $H_{\text{Sys}}^{\text{el}}$. Figure 3, for example, explains that four vibronic excitons will be found in a dimer, where each site possesses two vibronic levels (i.e., $\nu = 0$ and 1). The size of the Huang–Rhys factor is the key parameter governing the appropriate view of electronic structure. If the Huang–Rhys factor is small, then only the intersite coupling between the $\nu = 0$ states will be significant and $H_{\text{Sys}}^{\text{el}}$ is a good approximation. However, $H_{\text{Sys}}^{\text{vb}}$ is more appropriate when large mode displacements give rise to significant interactions between higher energy vibronic states ($\nu > 0$). Clearly, the two Hamiltonians differ fundamentally in their views of electronic structure. The central issue examined here is the possibility that one Hamiltonian is better able to explain the relaxation rates of both APC and CPC in a consistent way.

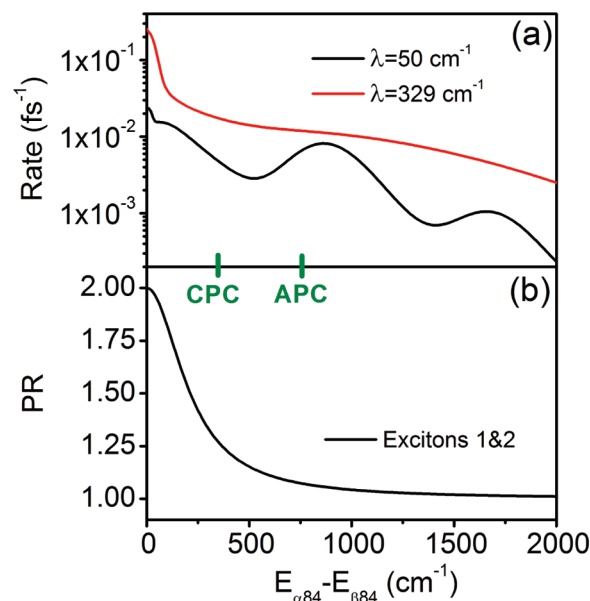
In the present analysis, the difference in site energies is viewed as the primary physical quantity distinguishing relaxation processes in APC and CPC. There may also be minor differences in the time scales of the bath and the reorganization energies in these two systems. However, the calculations presented below suggest it unlikely that differences in these characteristics of the bath justify the large disparity in kinetics. The parameters given in Table 1 are based on our previous analysis of spectroscopic measurements.^{24,25} It is true that the values of Λ_m and λ_m obtained by fitting spectroscopic signals will generally depend on the model employed. Therefore, effort is made to establish that the insights obtained below are robust within a physically reasonable range of parameter space.

Table 1. Empirical Parameters Obtained from Fitting of Spectroscopic Signals

parameter	APC	CPC
$E(\alpha_{84})$	16 060 cm^{-1}	16 240 cm^{-1}
$E(\beta_{84})$	15 300 cm^{-1}	15 890 cm^{-1}
$\Lambda^{-1}(\alpha_{84})$	296 fs	278 fs
$\Lambda^{-1}(\beta_{84})$	238 fs	327 fs
$\lambda(\alpha_{84})$	360 cm^{-1}	417 cm^{-1}
$\lambda(\beta_{84})$	235 cm^{-1}	304 cm^{-1}

**Figure 4.** Modified Redfield rate constants, K_{12} , computed using $H_{\text{Sys}}^{\text{el}}$. The time scale of the bath, which is equivalent at each site, is (a) 283 and (b) 100 fs. The intermolecular coupling and Huang–Rhys factor for the HOOP mode are given in Table 2. At $\lambda < 100 \text{ cm}^{-1}$, the 800 cm^{-1} mode promotes well-defined rate enhancements when the difference in site energies, $E_{\alpha_{84}} - E_{\beta_{84}}$, is near 775 and 1600 cm^{-1} . Panels (a) and (b) display the logarithm (base 10) of K_{12} .

IIIA. Purely Electronic Excitons. Modified Redfield rate constants are displayed with respect to the site reorganization energies, λ , and the difference in site energies, $E_{\alpha_{84}} - E_{\beta_{84}}$, in Figure 4. In the interest of obtaining general physical insights, the reorganization energies are constrained to be the same for both pigments. The calculation reveals significant differences in the relaxation processes computed at small and large values of the reorganization energy. At $\lambda < 100 \text{ cm}^{-1}$, the calculation finds well-defined rate enhancements when $E_{\alpha_{84}} - E_{\beta_{84}}$ is equal to 775 and 1600 cm^{-1} , which reflects participation of the HOOP coordinate as a promoting mode. The rate enhancement computed near 1600 cm^{-1} underscores the aforementioned ability of modified Redfield theory to describe nonradiative transitions involving the exchange of multiple excitation quanta with the bath. The well-defined rate enhancements calculated at $\lambda < 100 \text{ cm}^{-1}$ broaden and eventually disappear as the reorganization energy increases. Effectively, the reorganization energy inflates the “bandwidth” of the vibronic relaxation channel until it is no

**Figure 5.** (a) Modified Redfield rate constant, K_{12} , computed using $H_{\text{Sys}}^{\text{el}}$ and the parameters in Table 2. The value of the reorganization energy, which is equivalent at the two sites, is given in the Figure legend. (b) Participation ratio computed using eq 14. Also indicated are the empirically obtained differences in the site energies for APC and CPC. (See Table 1.)

longer well-localized at particular values of $E_{\alpha_{84}} - E_{\beta_{84}}$. The calculation in Figure 4 is repeated with different bath correlation times to make clear that this physical insight holds under reasonable variation of the parameters. To be consistent with our experiments,^{24,25} both calculations are conducted in the slow modulation regime where (approximately) Gaussian line shapes are obtained.⁵³ The spectral density, $C_m^{\text{OD}}(\omega)$, concentrates more of its amplitude at $\omega < k_B T$ with $\Lambda^{-1} = 283 \text{ fs}$ than with $\Lambda^{-1} = 100 \text{ fs}$. For this reason, large rate constants are predicted in Figure 4a even when $\lambda < 200 \text{ cm}^{-1}$ (i.e., with weak system–bath coupling). In the range of $E_{\alpha_{84}} - E_{\beta_{84}}$ relevant to APC and CPC, similar results are obtained for both values of Λ , which suggests that these physical insights are robust.

Figure 5 presents 1D slices through the contour plot in Figure 4. This representation makes it clear that the rate enhancement associated with the HOOP coordinate is insensitive to the value of $E_{\alpha_{84}} - E_{\beta_{84}}$ when the reorganization energy is near that found experimentally. Most importantly, the rate decreases monotonically with $E_{\alpha_{84}} - E_{\beta_{84}}$ at realistic values of the site reorganization energies, which are most assuredly $>100 \text{ cm}^{-1}$ because the measured spectroscopic line widths are at least 500 cm^{-1} . For example, in contrast with the observed kinetics, the calculation predicts that the relaxation rate is 1.5 times faster in CPC than it is in APC with $\lambda = 329 \text{ cm}^{-1}$. Insight into this behavior is obtained using the participation ratio⁵

$$PR_a = \frac{1}{\sum_{m=1}^N \phi_{am}^4} \quad (14)$$

PR_a is equal to 1 and 2 in the limit of fully localized and delocalized states, respectively. As should be expected, Figure 5 predicts that the excitons become more localized as $E_{\alpha_{84}} - E_{\beta_{84}}$

increases. The 1.07 value of PR_a computed at $E_{\alpha 84} - E_{\beta 84} = 760 \text{ cm}^{-1}$ suggests that the Förster energy transfer mechanism should be a good approximation for APC. In fact, the Förster energy transfer mechanism is known to provide an accurate description of

Table 2. Parameters Used in Calculations

parameter	value
$E(\alpha 84)$	varied
$E(\beta 84)$	$15\,595 \text{ cm}^{-1}$
$J_{\alpha 84, \beta 84}^a$	-150 cm^{-1}
$\Lambda^{-1}(\alpha 84) = \Lambda^{-1}(\beta 84)^b$	283 fs
$\lambda(\alpha 84) = \lambda(\beta 84)^b$	329 cm^{-1}
ω^c	800 cm^{-1}
S^c	0.125

^a Parameter of eqs 2 and 9. ^b Parameter of eq 3 obtained as averages of the empirical values given in Table 1. ^c Parameter of eqs 4 and 9.

the dynamics in CPC where, according to $H_{\text{Sys}}^{\text{el}}$, the tendency for wave function delocalization is even greater ($PR_a = 1.27$).³⁰

Overall, the simulations presented in this Section are inconsistent with dynamics measured in APC and CPC.^{24,25} Most important in reaching this conclusion is the model's prediction that, contrary to experimental observations, electronic relaxation is faster in CPC than in APC at realistic values of the reorganization energy (c.f., Figure 5). The calculations show that the transition loses sensitivity to the energy difference between the initial and final states when λ increases because of growth in the "bandwidth" of the vibronic relaxation channel, which is similar in magnitude to the spectroscopic line width. The calculated exciton sizes are also inconsistent with experiments. The calculations presented in Figure 5 suggest that the excited states of CPC are more delocalized than those of APC, whereas the opposite behavior is found experimentally.^{24,25}

It should be emphasized that the insights obtained here are based on a physically motivated correlation function, $C_m^{\text{UD}}(\omega)$,

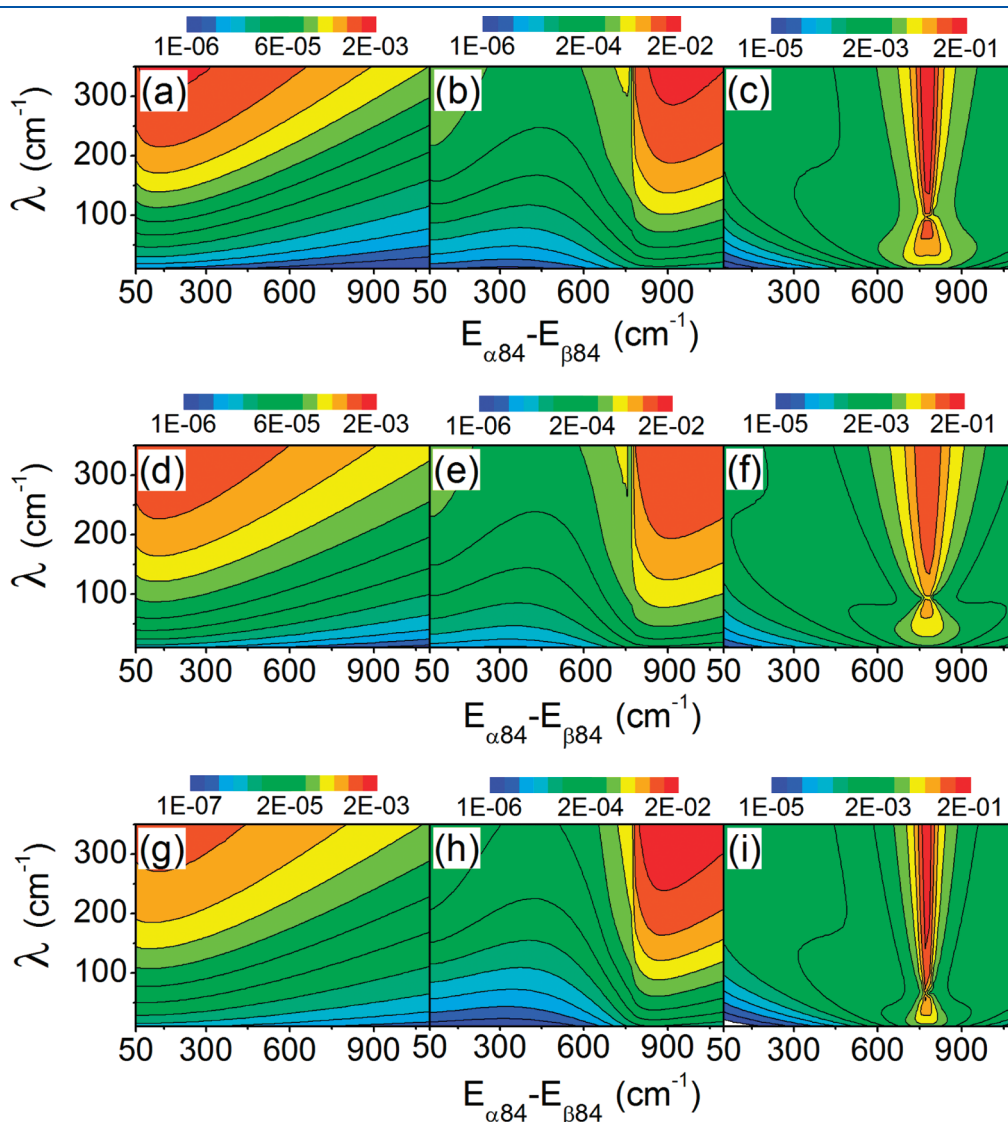


Figure 6. Modified Redfield rate constants computed using $H_{\text{Sys}}^{\text{vb}}$. Calculated rate constants include K_{12} (left column), K_{13} (middle column), and K_{23} (right column). (a–c) All parameters of Table 2 are used. (d–f) All parameters of Table 2 are used except that Λ^{-1} is set equal to 100 fs. (g–i) All parameters of Table 2 are used except that $S = 0.05$. In contrast with calculations based on $H_{\text{Sys}}^{\text{el}}$, well-defined rate enhancements are predicted near $E_{\alpha 84} - E_{\beta 84} = \hbar\omega$ at realistic values of the reorganization energy ($\lambda > 100 \text{ cm}^{-1}$). All panels display the logarithm (base 10) of the rate constants.

which treats only the intramolecular HOOP mode explicitly. Higher frequency bond stretching modes are observed in the resonance Raman spectra of phycocyanobilin.^{58–60} However, modes with frequencies greater than the exciton splitting will have little influence on the dynamics because such vibronic relaxation channels would be energetically “uphill”. In principle, the underdamped modes detected near 250 cm^{−1} in both APC and CPC can serve as promoting modes.^{24,37} However, the nonradiative transition in APC would then deposit roughly three quanta of energy (i.e., total of 750 cm^{−1}) in the acceptor state. In this scenario, the coordinate would require an exceptionally large displacement in order for it to constitute the dominant relaxation channel. More importantly, a relaxation mechanism involving modes near 250 cm^{−1} would suggest that CPC possesses a faster relaxation rate than APC because of its smaller exciton splitting (i.e., only two quanta of energy would be deposited in the acceptor state).

IIIB. Vibronic Excitons. In this Section, rate constants are computed with $H_{\text{Sys}}^{\text{vb}}$ to address inconsistencies found when $H_{\text{Sys}}^{\text{el}}$ is employed. The vibronic exciton Hamiltonian matrix is given by

$$H_{\text{Sys}}^{\text{vb}} = \begin{pmatrix} E_{\alpha 84} & 0 & V_{00} & V_{01} \\ 0 & E_{\alpha 84} + \hbar\omega & V_{10} & V_{11} \\ V_{00} & V_{10} & E_{\beta 84} & 0 \\ V_{01} & V_{11} & 0 & E_{\beta 84} + \hbar\omega \end{pmatrix} \quad (15)$$

where $V_{mn} = J_{\alpha 84, \beta 84} \langle 0|m \rangle \langle 0|n \rangle$. The expansion of vibronic states, $|m, \nu\rangle$, in the HOOP mode is truncated at $\nu = 1$ because the electronic origin dominates the vibronic progressions in APC and CPC (i.e., relatively small Huang–Rhys factors).^{24,25} This choice of basis is additionally well-suited for interpretation of our experiments because the laser pulses utilized in these studies primarily excited electronic states with resonances on the lower energy portion of the linear absorption spectra. Off-diagonal elements corresponding to different vibronic levels at a particular site are set equal to zero in $H_{\text{Sys}}^{\text{vb}}$. A more sophisticated treatment of these elements, which is beyond the scope of the present work, would capture the effects of intramolecular vibrational energy redistribution (IVR). As in Section IIIA, the dimensionless displacement of the HOOP coordinate is set equal to 0.5. However, vibronic coupling now directly controls the magnitudes of intermolecular interactions through the couplings in $H_{\text{Sys}}^{\text{vb}}$.

Figure 6 displays the rate constants K_{12} , K_{13} , and K_{23} as a function of $E_{\alpha 84} - E_{\beta 84}$ and the site reorganization energies, which are taken to be equivalent for both pigments. The rate, K_{12} , decreases monotonically as the difference in site energies increases, which is similar to the behavior shown in Figure 4. This similarity should be expected because the two lowest energy excitons have small contributions from excited vibronic levels when $E_{\alpha 84} - E_{\beta 84} < \hbar\omega$ (c.f., Figure 3). In contrast, K_{13} exhibits a steep rate increase when the nature of the nonradiative transition changes from intrasite to intersite at $E_{\alpha 84} - E_{\beta 84} = \hbar\omega$; intersite transitions are obtained at $E_{\alpha 84} - E_{\beta 84} > \hbar\omega$. As mentioned above, the intrasite transitions are slow because $H_{\text{Sys}}^{\text{vb}}$ neglects IVR processes on the individual pigments. Finally, K_{23} possesses a marked enhancement in the electronic population transfer rate at $E_{\alpha 84} - E_{\beta 84} = \hbar\omega$. At this value of $E_{\alpha 84} - E_{\beta 84}$, the excited vibronic level of the $\beta 84$ pigment is degenerate with the electronic origin of the $\alpha 84$ pigment, thereby promoting exciton

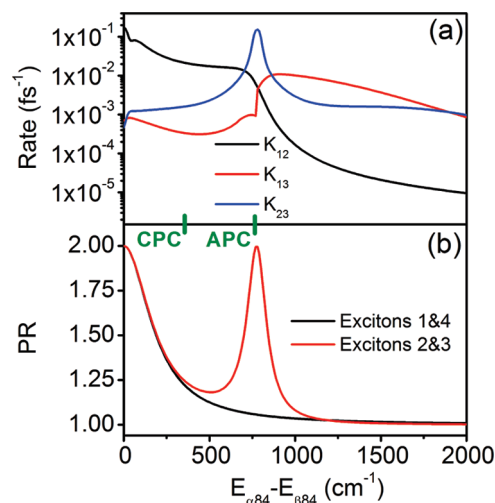


Figure 7. (a) Modified Redfield rate constants computed using $H_{\text{Sys}}^{\text{vb}}$ and the parameters in Table 2. Color coding for the K_{12} , K_{13} , and K_{23} rate constants is defined in the Figure legend. (b) Participation ratios calculated using eq 16. Also indicated are the empirically obtained differences in the site energies for APC and CPC. (See Table 1.)

delocalization through the V_{01} elements in $H_{\text{Sys}}^{\text{vb}}$. The behavior of K_{23} is distinct from that shown in Figure 4, where the HOOP mode is regarded as part of the bath in that a well-defined enhancement is found near $E_{\alpha 84} - E_{\beta 84} = \hbar\omega$ even at large values of the site reorganization energies. Profiles of these three rate constants at realistic values of λ are shown in Figure 7. To ensure that these physical insights are robust, Figure 6 presents rate constants calculated with a shorter bath time scale, $\Lambda^{-1} = 100 \text{ fs}$, and smaller Huang–Rhys factor, $S = 0.05$. The shorter bath correlation time has little effect on K_{12} and K_{13} , whereas K_{23} is slightly smaller and does not peak as sharply at $E_{\alpha 84} - E_{\beta 84} = \hbar\omega$. The decrease in S also has a minor influence on the calculated rate constants; the pronounced rate enhancement in K_{23} persists when $E_{\alpha 84} - E_{\beta 84} = \hbar\omega$.

Spatial overlap in excitons 2 and 3 is at the root of the rate enhancement predicted in APC. Exciton sizes are quantified using a participation ratio valid for vibronic excitons

$$PR_a = \frac{1}{\sum_{m=1}^N \left(\sum_{\nu=0} \phi_{a, m\nu}^2 \right)^2} \quad (16)$$

As in eq 14, PR_a is, respectively, equal to 1 and 2 for fully localized and delocalized states. Figure 7b shows that PR_a maximizes near $E_{\alpha 84} - E_{\beta 84} = \hbar\omega$ when the excited vibronic level at the $\beta 84$ pigment comes into degeneracy with the electronic origin of $\alpha 84$. This delocalization mechanism contrasts with the common view that heterogeneity in molecular sites (i.e., diagonal disorder) can only suppress exciton delocalization. The present calculations show that special circumstances may arise in which large vibronic couplings actually promote delocalization. As illustrated in Figure 3b, the key to this delocalization mechanism is the resonance in (staggered) vibronic transitions with large Franck–Condon factors made possible by heterogeneity in the site energies.

The most important aspect of these calculations is that a clear enhancement in the K_{23} of APC is predicted by invoking its

experimentally established difference in site energies. Moreover, unlike the prediction of the purely electronic exciton model, the present rate enhancement persists at realistic site reorganization energies. *We therefore suggest that $H_{\text{Sys}}^{\text{vb}}$ successfully pinpoints the mechanism responsible for ultrafast population flow in APC while simultaneously justifying slower electronic relaxation in CPC.* In addition to explaining the difference in kinetics, the vibronic exciton model yields exciton sizes consistent with the transient absorption anisotropies observed in both systems, which indicate greater wave function delocalization in APC. We envision that exciton delocalization in APC will be fairly delicate because the intermolecular couplings are (slightly) smaller than the site reorganization energies (e.g., $V_{01} = -60 \text{ cm}^{-1}$ when $S = 0.5$). One possibility is that the vibronic exciton delocalization mechanism operates for only a short amount of time following photoexcitation before solvation processes break the degeneracy depicted in Figure 3b and trap the excitation on the lower energy $\beta 84$ site. Simulations conducted using a model capable of capturing self-trapping dynamics will be needed to address this issue.^{6,61}

IV. CONCLUSIONS

The main conclusion of this Article is that the behavior predicted by the vibronic exciton model is more consistent with experimental results for APC and CPC than that obtained when the HOOP mode is regarded to be a part of the spectral density. Most important to this conclusion is the result that well-defined rate enhancements persist near $E_{\alpha 84} - E_{\beta 84} = \hbar\omega$ at realistic values of the site reorganization energies ($\lambda > 100 \text{ cm}^{-1}$). As shown in Figures 5 and 7, only with the vibronic exciton model are faster electronic relaxation processes predicted in APC when $\lambda > 100 \text{ cm}^{-1}$. These rate enhancements originate in a vibronic exciton delocalization mechanism, which takes hold primarily in APC (c.f., Figure 3). Extensions of the model presented here should develop strategies for simulating the IVR processes taking place subsequent to electronic population transfer. The role of fast, solvation-driven exciton self-trapping should also be investigated. It is hoped that our experiments and the interpretation offered here will motivate rigorous theoretical studies of these systems. APC and CPC are excellent models for studying vibronic effects on exciton sizes and energy transport, which are generally quite difficult to pinpoint experimentally.

An important broader implication of this work is that vibronic coupling may be more intimately connected to energy transfer in photosynthetic complexes than it is usually given credit for. Vibronic effects similar to those investigated here may indeed promote exciton delocalization in a wider variety of systems. As discussed in Section IIIB, the key ingredient underlying this mechanism of wave function delocalization is a degeneracy in staggered vibronic levels at different pigments made possible by diagonal disorder. In these situations, purely electronic exciton models underestimate exciton sizes because they see heterogeneity among sites as only a localizing influence. Exciting new research applies measures of entanglement developed in the field of quantum information to light-harvesting proteins.^{61–65} In this context, it will be interesting to investigate the role of the vibronic effects on quantum entanglement in these and other systems.

■ APPENDIX

This Appendix presents the multimode harmonic BO model employed in this work. We summarize the key equations specific

to the systems investigated in this Article. The general formulation of the BO model has been discussed in detail elsewhere.^{5,43,53} Hamiltonians describing the bath and system–bath interaction, which are components of eq 1, are given by⁴³

$$H_{\text{Bath}} = \frac{1}{2} \sum_j \left[\frac{p_j^2}{M_j} + M_j \bar{\Omega}_j^2 Q_j^2 \right] + \frac{1}{2} \sum_{\alpha} \left[\frac{p_{\alpha}^2}{m_{\alpha}} + m_{\alpha} \bar{\omega}_{\alpha}^2 \left(q_{\alpha} - \sum_j \frac{z_{j\alpha}}{m_{\alpha} \bar{\omega}_{\alpha}^2} Q_j \right)^2 \right] \quad (\text{A1})$$

$$H_{\text{Sys} - \text{Bath}} = \sum_m \sum_j \bar{h}_{mj} Q_j B_m^{\dagger} B_m \quad (\text{A2})$$

Both H_{Bath} and $H_{\text{Sys} - \text{Bath}}$ distinguish between the primary, Q_j , and secondary, q_{α} , oscillators. Here $P_j, \bar{\Omega}_j, M_j$ ($p_{\alpha}, \bar{\omega}_{\alpha}, m_{\alpha}$) are the momenta, frequencies, and masses of the primary (secondary) coordinates. The primary oscillators couple linearly to electronic excitations at the pigment sites, m_j , with the coupling strength $\bar{h}_{mj} = M_j \bar{\Omega}_j^2 d_{mj}$, where $d_{mj} (M_j \bar{\Omega}_j^2)^{1/2}$ is the dimensionless displacement in Q_j from its equilibrium position. The secondary oscillators interact with the primary oscillators through the coupling parameter, $z_{j\alpha}$, but do not influence the electronic structure of the system directly.

It is useful to point out two fundamental assumptions made in the present applications to APC and CPC, which distinguish it from a more general treatment. First, it is assumed that different pigment sites do not interact with the same primary oscillator (i.e., no shared modes). This aspect of the model is reasonable given that the intermolecular distances within the dimers of both APC and CPC are $\sim 2 \text{ nm}$. Moreover, contributions from shared modes were ruled out in our previous experimental investigations.^{24–26} Second, we assume that the primary oscillators influence the site energies in $H_{\text{Sys}}^{\text{el}}$ and $H_{\text{Sys}}^{\text{vb}}$ but not the Coulombic couplings. This approximation is motivated, in part, by the limited empirical parameters available. However, it can also be justified by the relatively small size of J_{mn} ($\sim 150 \text{ cm}^{-1}$) compared with the E_m ($\geq 15\,300 \text{ cm}^{-1}$). This second assumption is implicit in the form of $H_{\text{Sys} - \text{Bath}}$ given in eq A2.

The spectral density at pigment site m is conveniently written as

$$K''_m(\omega) = -\frac{\bar{h}_{mj}^2}{2} \sum_j \int_{-\infty}^{\infty} dt \exp(i\omega t) \langle [Q_j(t), Q_j(0)] \rangle \quad (\text{A3})$$

by assuming that the primary oscillators are uncorrelated. Similarly, the spectral density of the secondary oscillators is given by

$$K''_{\alpha}(\omega) = -\frac{1}{2} \int_{-\infty}^{\infty} dt \exp(i\omega t) \langle [q_{\alpha}(t), q_{\alpha}(0)] \rangle \quad (\text{A4})$$

With these spectral densities in hand, closed forms of the correlation functions appropriate for the treatment of intermolecular and intramolecular modes can be found in the limits of small and large friction imposed on the primary oscillators, Q_j , by the secondary oscillators, q_{α} . The amount of friction, in turn, determines the rate at which thermally driven fluctuations

of the site energies relax. The form of the spectral density, $C''_m(\omega)$, is governed by the relative sizes of the oscillator frequencies, Ω_j , and the friction

$$\gamma_j(\omega) = \frac{1}{M_j\omega} \sum_{\alpha} z_{j\alpha}^2 K''_{\alpha}(\omega) \quad (\text{A5})$$

Limiting forms of $C''_m(\omega)$ are conveniently found by assuming that $\gamma_j(\omega)$ is frequency-independent, which signifies that the thermal motions of the bath are fast compared with those of the Q. When $\gamma_j \gg \Omega_j$, the spectral density is given by

$$C''_j(\omega) = 2\lambda'_j \frac{\omega\Lambda_j}{\omega^2 + \Lambda_j^2} \quad (\text{A6})$$

where $\lambda'_j = (2M_j\bar{\Omega}_j^2)^{-1}$ and $\Lambda_j = \bar{\Omega}_j^2/\gamma_j$. In the opposite limit, the spectral density is written as

$$C''_j(\omega) = \frac{1}{2M_j\bar{\Omega}_j} [\delta(\omega - \Omega_j) - \delta(\omega + \Omega_j)] \quad (\text{A7})$$

Equations 3 and 4 are, respectively, obtained by combining the overdamped and underdamped versions of $C''_j(\omega)$ with eq A3.

Intermolecular and intramolecular modes involving the phycocyanobilin pigments of APC and CPC are well-described in the overdamped and underdamped limits of the BO model, respectively. Liquid water, which likely makes a significant contribution to the fastest solvation processes in these proteins,^{24,25,66} has a low-frequency Raman spectrum dominated by nuclear motions at frequencies $<200 \text{ cm}^{-1}$. In contrast, strongly coupled intramolecular modes of phycocyanobilin pigments are found throughout the fingerprint region (e.g., $500\text{--}2000 \text{ cm}^{-1}$).^{58–60} In addition to possessing lower frequencies, the intermolecular modes of the environment (i.e., solvent) that couple to the pigments (i.e., solute) generally also have strong interactions with secondary solvation layers (i.e., large $z_{j\alpha}$ in eq A5) and therefore satisfy the limit $\gamma_j \gg \Omega_j$. The intramolecular modes of the phycocyanobilins (e.g., stretching and bending above 500 cm^{-1}) are generally underdamped (i.e., narrow line widths are observed in Raman spectra) because they have relatively weak interactions with the environments surrounding the pigments.

ACKNOWLEDGMENT

This material is based on work supported by the National Science Foundation under CHE-0952439. J.M.W. acknowledges the Institute for the Environment at the University of North Carolina for a graduate fellowship. We thank the anonymous reviewer for helpful suggestions.

REFERENCES

- (1) van Amerongen, H.; Valkunas, L.; van Grondelle, R. *Photosynthetic Excitons*; World Scientific: Singapore, 2000.
- (2) Grover, M.; Silbey, R. J. *J. Chem. Phys.* **1971**, *54*, 4843.
- (3) De Boer, S.; Wiersma, D. A. *Chem. Phys.* **1989**, *131*, 135.
- (4) Rebentrost, P.; Mohseni, M.; Kassal, L.; Lloyd, S.; Aspuru-Guzik, A. *New J. Phys.* **2009**, *11*, 033003:1.
- (5) Abramavicius, D.; Palmieri, B.; Voronine, D. V.; Sanda, F.; Mukamel, S. *Chem. Rev.* **2009**, *109*, 2350.
- (6) Tanimura, Y. *J. Phys. Soc. Jpn.* **2006**, *75*, 082001.
- (7) Ishizaki, A.; Fleming, G. R. *J. Chem. Phys.* **2009**, *130*, 234110.
- (8) Fassiolli, F.; Nazir, A.; Olaya-Castro, A. *J. Phys. Chem. Lett.* **2010**, *1*, 2139.

- (9) Cina, J. A.; Fleming, G. R. *J. Phys. Chem. A* **2004**, *108*, 11196.
- (10) Mancal, T.; Nemeth, A.; Milota, F.; Lukes, V.; Kauffmann, H. F. *J. Chem. Phys.* **2010**, *132*, 184515.
- (11) Reineker, P.; Suprit, C.; Warns, C.; Barvik, I. *J. Lumin.* **2004**, *108*, 149.
- (12) Renger, T. *Photosynth. Res.* **2009**, *102*, 471.
- (13) Eisfeld, A.; Briggs, J. S. *Chem. Phys.* **2002**, *281*, 61.
- (14) Seibt, J.; Marquetand, P.; Engel, V.; Chen, Z.; Dehm, V.; Würthner, F. *Chem. Phys.* **2006**, *328*, 354.
- (15) Roden, J.; Schulz, G.; Eisfeld, A.; Briggs, J. J. *Chem. Phys.* **2009**, *131*, 044909.
- (16) McRae, E. G.; Siebrand, W. J. *Chem. Phys.* **1964**, *41*, 905.
- (17) Philpott, M. R. *J. Chem. Phys.* **1967**, *47*, 4437.
- (18) Spano, F. C. *Acc. Chem. Res.* **2010**, *43*, 429.
- (19) Ahn, T.-S.; Müller, A. M.; Al-Kaysi, R. O.; Spano, F. C.; Norton, J. E.; Beljonne, D.; Brédas, J.-L.; Bardeen, C. J. *J. Chem. Phys.* **2008**, *128*, 054505.
- (20) Schwoerer, M.; Wolf, H. C. *Organic Molecular Solids*; Wiley-VCH: Weinheim, Germany, 2007.
- (21) Jonas, D. M.; Lang, M. J.; Nagasawa, Y.; Joo, T.; Fleming, G. R. *J. Phys. Chem.* **1996**, *100*, 12660.
- (22) Arnett, D. C.; Moser, C. C.; Dutton, P. L.; Scherer, N. F. *J. Phys. Chem. B* **1999**, *103*, 2014.
- (23) Wynne, K.; Haran, G.; Reid, G. D.; Moser, C. C.; Dutton, P. L.; Hochstrasser, R. M. *J. Phys. Chem.* **1996**, *100*, 5140.
- (24) Womick, J. M.; Moran, A. M. *J. Phys. Chem. B* **2009**, *113*, 15747.
- (25) Womick, J. M.; Moran, A. M. *J. Phys. Chem. B* **2009**, *113*, 15771.
- (26) Womick, J. M.; Miller, S. A.; Moran, A. M. *J. Chem. Phys.* **2010**, *133*, 024507.
- (27) Brejc, K.; Ficner, R.; Huber, R.; Steinbacher, S. *J. Mol. Biol.* **1995**, *249*, 424.
- (28) Wang, X.-Q.; Li, L.-N.; Chang, W.-R.; Zhang, J.-P.; Gui, L.-L.; Guo, B.-J.; Liang, D.-C. *Acta Crystallogr.* **2001**, *D57*, 784.
- (29) Gillbro, T.; Sharkov, A. V.; Kryukov, I. V.; Khoroshilov, E. V.; Kryukov, P. G.; Fischer, R.; Scheer, H. *Biochim. Biophys. Acta* **1993**, *1140*, 321.
- (30) Debreczeny, M. P.; Sauer, K.; Zhou, J.; Bryant, D. A. *J. Phys. Chem.* **1995**, *99*, 8420.
- (31) Sharkov, A. V.; Kryukov, I. V.; Khoroshilov, E. V.; Kryukov, P. G.; Fischer, R.; Scheer, H.; Gillbro, T. *Chem. Phys. Lett.* **1992**, *191*, 633.
- (32) Edington, M. D.; Riter, R. E.; Beck, W. F. *J. Phys. Chem.* **1996**, *100*, 14206.
- (33) Riter, R. E.; Edington, M. D.; Beck, W. F. *J. Phys. Chem. B* **1997**, *101*, 2366.
- (34) Edington, M. D.; Riter, R. E.; Beck, W. F. *J. Phys. Chem.* **1995**, *99*, 15699.
- (35) Edington, M. D.; Riter, R. E.; Beck, W. F. *J. Phys. Chem. B* **1997**, *101*, 4473.
- (36) Riter, R. E.; Edington, M. D.; Beck, W. F. *J. Phys. Chem.* **1996**, *100*, 14198.
- (37) Zhang, J. M.; Shiu, Y. J.; Hayashi, M.; Liang, K. K.; Chang, C. H.; Gulbinas, V.; Yang, C. M.; Yang, T.-S.; Wang, H. Z.; Chen, Y.-T.; Lin, S. H. *J. Phys. Chem. A* **2001**, *105*, 8878.
- (38) Zhang, J. M.; Zhao, F. L.; Zheng, X. G.; Wang, H. Z.; Yang, T.-S.; Hayashi, M.; Lin, S. H. *J. Photochem. Photobiol., B* **1999**, *53*, 128.
- (39) Zhang, W. M.; Meier, T.; Chernyak, V.; Mukamel, S. *J. Chem. Phys.* **1998**, *108*, 7763.
- (40) Yang, M.; Fleming, G. R. *Chem. Phys.* **2002**, *282*, 163.
- (41) Redfield, A. G. *Adv. Magn. Reson.* **1965**, *1*, 1.
- (42) Förster, T. *Ann. Phys.* **1948**, *437*, 55.
- (43) Abramavicius, D.; Mukamel, S. *Chem. Rev.* **2004**, *104*, 2073.
- (44) Spano, F. C. *Annu. Rev. Phys. Chem.* **2006**, *57*, 217.
- (45) Zhuang, W.; Hayashi, T.; Mukamel, S. *Angew. Chem.* **2009**, *48*, 3750.
- (46) Lim, S.-H.; Bjorklund, T. G.; Spano, F. C.; Bardeen, C. J. *Phys. Rev. Lett.* **2004**, *92*, 107402:1.
- (47) West, B. A.; Womick, J. M.; McNeil, L. E.; Tan, K. J.; Moran, A. M. *J. Phys. Chem. C* **2010**, *114*, 10580.

- (48) Sanematu, T. *J. Phys. Soc. Jpn.* **1976**, *43*, 600.
- (49) Sanematu, T.; Mizuno, Y. *J. Phys. Soc. Jpn.* **1976**, *40*, 1733.
- (50) Linnanto, J. M.; Korppi-Tommola, J. E. I. *Chem. Phys.* **2009**, *357*, 171.
- (51) Spano, F. C.; Meskers, S. C. J.; Hennebicq, E.; Beljonne, D. *J. Am. Chem. Soc.* **2007**, *129*, 7044.
- (52) Spano, F. C.; Silvestri, L.; Spearman, P.; Raimondo, L.; Tavazzi, S. *J. Chem. Phys.* **2007**, *127*, 184703:1.
- (53) Mukamel, S. *Principles of Nonlinear Optical Spectroscopy*; Oxford University Press: New York, 1995.
- (54) Holstein, T. *Ann. Phys.* **1959**, *8*, 325.
- (55) Myers, A. B.; Mathies, R. A. *J. Chem. Phys.* **1984**, *81*, 1552.
- (56) Eisfeld, A.; Briggs, J. S. *Chem. Phys.* **2006**, *324*, 376.
- (57) Roden, J.; Eisfeld, A.; Briggs, J. S. *Chem. Phys.* **2008**, *352*, 258.
- (58) Szalontai, B.; Gombos, Z.; Csizmadia, V.; Csatorday, K.; Lutz, M. *Biochemistry* **1989**, *28*, 6467.
- (59) Szalontai, B.; Gombos, Z.; Csizmadia, V.; Bagyinka, C.; Lutz, M. *Biochemistry* **1994**, *33*, 11823.
- (60) Andel, F., III; Murphy, J. T.; Haas, J. A.; McDowell, M. T.; van der Hoef, I.; Lugtenburg, J.; Lagarias, J. C.; Mathies, R. A. *Biochemistry* **2000**, *39*, 2667.
- (61) Ishizaki, A.; Fleming, G. R. *New J. Phys.* **2010**, *12*, 055004.
- (62) Sarovar, M.; Ishizaki, A.; Fleming, G. R.; Whaley, K. B. *Nat. Phys.* **2010**, *6*, 462.
- (63) Mukamel, S. *J. Chem. Phys.* **2010**, *132*, 241105.
- (64) Thorwart, M.; Eckel, J.; Reina, J. H.; Nalbach, P.; Weiss, S. *Chem. Phys. Lett.* **2009**, *478*, 234.
- (65) Hossein-Nejad, H.; Scholes, G. D. *New J. Phys.* **2010**, *12*, 065045.
- (66) Homoelle, B. J.; Edington, M. D.; Diffey, W. M.; Beck, W. F. *J. Phys. Chem. B* **1998**, *102*, 3044.